A new time dependent density functional algorithm for large systems and plasmons in metal clusters

Oscar Baseggio, Giovanna Fronzoni, and Mauro Stener

Citation: The Journal of Chemical Physics **143**, 024106 (2015); doi: 10.1063/1.4923368
View online: http://dx.doi.org/10.1063/1.4923368
View Table of Contents: http://scitation.aip.org/content/aip/journal/jcp/143/2?ver=pdfcov
Published by the AIP Publishing

A new time dependent density functional algorithm for large systems and plasmons in metal clusters

Oscar Baseggio, Giovanna Fronzoni, and Mauro Stener[a)]
Dipartimento di Scienze Chimiche e Farmaceutiche, Università di Trieste, Via Giorgieri 1, 34127 Trieste, Italy

(Received 10 April 2015; accepted 22 June 2015; published online 10 July 2015)

A new algorithm to solve the Time Dependent Density Functional Theory (TDDFT) equations in the space of the density fitting auxiliary basis set has been developed and implemented. The method extracts the spectrum from the imaginary part of the polarizability at any given photon energy, avoiding the bottleneck of Davidson diagonalization. The original idea which made the present scheme very efficient consists in the simplification of the double sum over occupied-virtual pairs in the definition of the dielectric susceptibility, allowing an easy calculation of such matrix as a linear combination of constant matrices with photon energy dependent coefficients. The method has been applied to very different systems in nature and size (from H_2 to $[Au_{147}]^-$). In all cases, the maximum deviations found for the excitation energies with respect to the Amsterdam density functional code are below 0.2 eV. The new algorithm has the merit not only to calculate the spectrum at whichever photon energy but also to allow a deep analysis of the results, in terms of transition contribution maps, Jacob plasmon scaling factor, and induced density analysis, which have been all implemented. © *2015 AIP Publishing LLC*. [http://dx.doi.org/10.1063/1.4923368]

I. INTRODUCTION

The calculation of optical spectra for large molecules has become a routine task, thanks to efficient implementations of the Time Dependent Density Functional Theory (TDDFT) method. More specifically, various approaches are available in computer codes which allow the treatment of large molecular systems.

In particular, it is worth mentioning the "standard" quantum chemistry approach, where molecular Kohn-Sham (KS) orbitals are expanded as linear combination of atomic functions, and the TDDFT equations are recast to a diagonalization of a matrix Ω according to the density matrix formulation of Casida.[1] The problem consists in extracting a set of eigenvalues and eigenvectors of Ω, whose dimension is Nocc × Nvirt. Such method is efficiently implemented in many quantum chemistry codes, like, for example, Amsterdam Density Functional (ADF) code,[2–4] which takes advantages of the molecular symmetry (employing the Wigner-Eckart theorem for the TDDFT part), of the Davidson diagonalization algorithm, of efficient fitting techniques of the first order density through the use of auxiliary basis functions to improve matrix-vector multiplication within the Davidson algorithm, and finally of the parallelization of the code which can exploit modern supercomputer architectures. Despite all these efforts, it is very difficult to calculate valence photoabsorption spectra over a wide excitation energy range when very large systems are considered. In fact, the Davidson iterative algorithm is very efficient on large Ω matrices, but it is limited to the extraction of a relatively small number of lowest eigenvalues and eigenvectors; such diagonalization algorithm is generally employed in all the TDDFT codes which use the Casida method, like, for example, TURBOMOLE.[5]

Therefore, the Casida TDDFT algorithm remains very efficient on large systems only when few low energy transitions are extracted but cannot be employed in practice to calculate a photoabsorption spectrum over a wide energy range, often necessary for a complete simulation of an experiment. Of course as the molecule/cluster size increases such problem will become more and more pathological, preventing any calculation of the spectrum. Moving from this practical consideration, it would be very appealing to find an alternative TDDFT algorithm to avoid the bottleneck of the Davidson diagonalization, capable to calculate the spectrum without limitations on the value of the maximum excitation energy.

Before describing the new algorithm, it is worth mentioning other recent alternative TDDFT strategies, which are promising for applications to large systems.

The first one is based on the explicit time-propagation technique. This scheme was introduced in the seminal work of Yabana and Bertsch[6] and is now implemented usually over real space grids, like in the OCTOPUS program,[7] which has been recently applied to study the photoabsorption of large biomolecules[8] and large metal clusters, clusters up to 147 atoms[9] and 263 atoms.[10]

The second one consists in a superoperator formulation of the TDDFT, which allows the calculation of the dynamical polarizability by means of a very efficient Lanczos method, implemented with plane waves basis set;[11] it has been applied to systems like C_{60}, C_{70}, zinc tetraphenylporphyrin, and chlorophyll a.[12–14] The Lanczos method is quite appealing for large systems since it furnishes the whole excitation spectrum, at variance with Davidson diagonalization which is limited to the lower part of the spectrum. A third very recent scheme has been developed by Grimme and consists in a simplified Tamm Dancoff Approximation (TDA)[15] and TDDFT,[16] while a linear-scaling TDDFT has been developed by Zuehlsdorff.[17]

a)e-mail: stener@univ.trieste.it

A very promising recent method for large systems is the TDDFT time-propagation with Transition Contribution Map (TCM) by Häkkinen,[18] which has been employed to calculate the spectrum of clusters containing up to 314 gold atoms protected by ligands. Very recently, Nobusada has developed a massively parallel implementation of TDDFT based on real-time and real-space,[19] which allowed to consider clusters containing up to 1414 gold atoms.[20] It is worth noting that each of these algorithms has its different pros and cons which must be taken into account. In particular, the Casida algorithm suffers for the already mentioned problem of extracting of a large number of eigenvalues, but it has the great advantage to allow a very detailed assignment of the spectral features in terms of one-electron (1h1p) excited configurations. On the other hand, the TDDFT algorithms based on the time-evolution allow the calculation of the spectrum on a wide energy range without any problem; however, they do not give information regarding the nature of the transitions involved in the spectral feature. The only possibility is the inspection of the first order perturbed density whose nature is useful for a qualitative description but the information gained is too limited to allow a detailed assignment in terms of electronic transitions. At the moment, to the best of our knowledge, the only method which does not suffer energy limitation and is able to give a detailed assignment is the TDDFT time-propagation with TCM by Häkkinen.[18]

Despite already Linear Response (LR) TDDFT implemented codes, it is worth mentioning also the subsystem formulation of LR-TDDFT,[21,22] which is a very promising new idea for future applications on very large systems.

Finally, it must be considered that also the development of highly parallel *ab initio* and density functional theory (DFT) codes like NWCHEM[23] is an alternative way to describe large systems with respect to the proposal of new TDDFT algorithms. This way appears very practical, thanks to availability of massively parallel supercomputers.

In the present work, we propose a new TDDFT algorithm for the efficient calculation of photoabsorption spectra without the need of the diagonalization and therefore at any given energy. The necessary approximations introduced in the scheme can be safely kept under control. Moreover, the present algorithm allows a detailed analysis of the spectrum both in terms of 1h1p excited configuration which can be represented by TCM as well as in terms of the first order perturbed density. The method has been implemented within the ADF suite of codes and has been parallelized with standard Message Passing Interface (MPI); therefore, it is suitable to run on very large supercomputers.

II. THEORETICAL METHOD AND IMPLEMENTATION

The first requirement of the new algorithm must be to avoid the diagonalization of the large Ω matrix, which is the main bottleneck of most implementations. This can be formally obtained if the photoabsorption spectrum $\sigma(\omega)$ is calculated point by point, from the imaginary part of the dynamical polarizability $\alpha(\omega)$,

$$\sigma(\omega) = \frac{4\pi\omega}{c}\mathrm{Im}\left[\alpha(\omega)\right]. \tag{1}$$

This expression is of practical interest when the polarizability is calculated for complex frequency, i.e., $\omega = \omega_r + i\omega_i$, where the real part ω_r is the scanned photon frequency (energy) and ω_i is the imaginary part which corresponds to a broadening of the discrete lines and can be interpreted as a pragmatic inclusion of the excited states finite lifetime. The introduction of a small imaginary part in the frequency is well established, for example, in the Lanczos method[11] and, more recently, in the damped response[24] formalism. This procedure introduces the arbitrary quantity ω_i and prevents the analysis of the spectrum by discrete lines. This is not a problem when the excited state density is so high that the analysis state-by-state would be impractical.

It will be shown in the following that it is possible to calculate efficiently the complex dynamical polarizability $\alpha(\omega)$ introducing some approximations. First, let us start with the definition

$$\alpha_{zz}(\omega) = \int \rho_z^{(1)}(\omega,\bar{r})\, z d\bar{r} \tag{2}$$

of the z-th diagonal term of the polarizability tensor, where $\rho_z^{(1)}(\omega,\bar{r})$ stands for the Fourier component of the given frequency of the first order time dependent induced density by the external time dependent scalar potential. For the calculation of the spectrum, the isotropic part of the tensor is actually extracted from the trace: $\alpha(\omega) = \frac{1}{3}\sum_{i=1}^{3}\alpha_{ii}(\omega)$, where the index i runs on the three components x, y, and z.

Following the TDDFT theory, the induced density can be calculated from the dielectric susceptibility $\chi_{KS}(\omega,\bar{r},\bar{r}')$ of a reference system of non-interacting electrons under the effect of an effective perturbing potential $V^z_{SCF}(\omega,\bar{r})$ sum of the external potential plus the Coulomb and the exchange-correlation (XC) response potential.

This is summarized by the following coupled linear equations:

$$\rho_z^{(1)}(\omega,\bar{r}) = \int \chi_{KS}(\omega,\bar{r},\bar{r}')\, V^z_{SCF}(\omega,\bar{r}')\, d\bar{r}', \tag{3}$$

$$V^z_{SCF}(\omega,\bar{r}) = V^z_{EXT}(\omega,\bar{r}) + \int \frac{\rho_z^{(1)}(\omega,\bar{r}')\, d\bar{r}'}{|\bar{r}-\bar{r}'|} + \left.\frac{\partial V_{XC}}{\partial\rho}\right|_{\rho^{(0)}} \rho_z^{(1)}(\omega,\bar{r}). \tag{4}$$

The Adiabatic Local Density Approximation (ALDA)[25] has been employed in expression (4) (XC kernel local in time and additionally also in space) and $V^z_{EXT}(\omega,\bar{r})$ corresponds in practice to the z dipole component. The present implementation is limited to ALDA and possible extensions to gradient corrected kernels are not expected to give any problem; on the other hand, in the present formulation, it is not possible to employ non-local kernels from hybrid functionals, as also specified after Equation (24).

Now, expressions (3) and (4) can be written in operatorial form

$$\rho_z^{(1)} = \chi_{KS} V^z_{SCF}, \tag{5}$$

$$V^z_{SCF} = V^z_{EXT} + K\rho_z^{(1)}, \tag{6}$$

where in expression (6), K stands for the sum of the Coulomb and the XC kernels,

$$K(\bar{r},\bar{r}') = K_C(\bar{r},\bar{r}') + K_{XC}(\bar{r},\bar{r}') = \frac{1}{|\bar{r}-\bar{r}'|} + \delta(\bar{r}-\bar{r}')\left.\frac{\partial V_{XC}}{\partial\rho}\right|_{\rho^{(0)}}. \quad (7)$$

Due to the linearity of (5) and (6), it is possible to eliminate V^z_{SCF} and to obtain an equation for $\rho^{(1)}_z$, which reads as

$$[1 - \chi_{KS}K]\,\rho^{(1)}_z = \chi_{KS}V^z_{EXT}. \quad (8)$$

Now, it is convenient to represent Equation (8) over a basis set and since the unknown term corresponds to the induced density, it is natural to choose the auxiliary density fitting functions f_μ as basis set. More precisely, it is even better to choose such basis as a subset of the fitting set, since the induced density will be affected mainly by valence orbitals so all the functions needed to fit the core density should be excluded without losing accuracy. This is true only when valence excitations are considered (like in the present work); if core electron excitations are considered, the algorithm remains valid, but the fitting functions must be selected in a different way, allowing flexibility in order to properly describe products between a core and a virtual orbital. With this representation $\rho^{(1)}_z(\omega,\vec{r}) = \sum_\mu^K f_\mu(\bar{r})\,b_\mu(\omega)$, the following non-homogeneous system of linear algebraic equations is obtained, which written in matrix formulation reads as

$$[\mathbf{S} - \mathbf{M}(\omega)]\,\mathbf{b} = \mathbf{d}. \quad (9)$$

In Equation (9), **S** is the overlap matrix between fitting functions, **b** is the unknown vector with the expansion coefficients $b_\mu(\omega)$ of $\rho^{(1)}_z$, and **d** is the frequency dependent vector corresponding to the known non-homogeneous term, whose components are

$$d_\mu = \langle f_\mu|\,\chi_{KS}(\omega)\,|z\rangle, \quad (10)$$

and finally, the elements of the frequency dependent matrix **M** are

$$M_{\mu\nu} = \langle f_\mu|\,\chi_{KS}(\omega)\,K\,|f_\nu\rangle. \quad (11)$$

Now, let us consider the computational effort needed to solve Equation (9): (i) the construction of the matrices **S**, **M**, and vector **d** and (ii) the resolution of linear system (9). First, consider the resolution of the linear system: it will scale with N^3 where N is the dimension of the matrix corresponding to the number of the fitting functions. Although this part scales with the third power, it will be shown that the dimension N can be kept in practice rather low, for example, for Au atom, 44 functions are enough to give accurate results, so a cluster of 1000 Au atoms will give a matrix of dimension 44 000, which is tractable with moderate efforts on a medium size computer cluster. This simple observation shows that as it concerns the linear system, the approach is competitive since it would allow to calculate much larger systems without the limitation of the Davidson algorithm, if a proper selection of the fit set is performed.

Let us now analyse the effort needed to build the frequency dependent $\mathbf{M}(\omega)$ matrix: apparently, this is a prohibitive task, since it should be repeated for each frequency. The original characteristic of the present new method is the introduction of a simple approximation which should enable the construction of $\mathbf{M}(\omega)$ as a linear combination of *frequency independent* matrices $\mathbf{G}^k$ with *frequency dependent* coefficients $s_k(\omega)$, with this expression,

$$\mathbf{M}(\omega) = \sum_k s_k(\omega)\,\mathbf{G}^k; \quad (12)$$

with this idea, a set of matrices $\{\mathbf{G}^k\}$ is calculated and stored only once at the beginning; then, the matrix $\mathbf{M}(\omega)$ is calculated very rapidly at each photon energy ω. To justify expression (12), we start with the expression of the KS dielectric susceptibility,[26]

$$\chi_{KS}(\omega,\bar{r},\bar{r}') = \sum_i^{Nocc}\sum_a^{Nvirt}\varphi_i(\bar{r})\,\varphi_a(\bar{r})\,\frac{4\varepsilon_{ia}}{\omega^2-\varepsilon^2_{ia}}\,\varphi_a(\bar{r}')\,\varphi_i(\bar{r}') = \sum_i^{Nocc}\sum_a^{Nvirt}\Theta_{ia}(\bar{r})\,\lambda_{ia}(\omega)\,\Theta_{ia}(\bar{r}') \quad (13)$$

in (13) we have assumed real KS occupied (φ_i) and virtual (φ_a) orbitals while $\varepsilon_{ia} = \varepsilon_a - \varepsilon_i$ are differences between virtual and occupied KS eigenvalues. Let us consider now carefully the right hand side of expression (13): the frequency dependence enters only in the $\lambda_{ia}(\omega)$ factor, which is "almost" constant for all the pairs of index *i*- and *a*- for which $\varepsilon_a - \varepsilon_i$ is almost constant. This happens when many ε_{ia} are close together, that is, when the density of "zero order" excitation energies is high. This important observation allows to profitably change the double sum in expression (13). In fact, let us consider the distribution of all the ε_{ia} on the excitation energy axis, like in Figure 1, and define an energy grid over this axis, starting from the minimum ε_{ia} which corresponds to $\varepsilon_{LUMO} - \varepsilon_{HOMO}$. The energy grid consists of P + 1 knots $\{E_k\}_{k=1,\ldots,P+1}$ and P intervals are defined as $I_k = [E_k, E_{k+1})$, $k = 1,\ldots,P$.

It is possible to change the double sum of previous Equation (13) as follows:

$$\chi_{KS}(\omega,\bar{r},\bar{r}') = \sum_{k=1}^{P}\sum_{\varepsilon_{ia}\in I_k}\Theta_{ia}(\bar{r})\,\lambda_{ia}(\omega)\,\Theta_{ia}(\bar{r}'). \quad (14)$$

The advantage of this new double sum is that, if the energy knots are dense enough, the values of ε_{ia} within each interval can be considered, with good approximation, almost constant and equal to the average $\overline{E}_i = \frac{E_i+E_{i+1}}{2}$: this allows to bring the $\lambda_{ia}(\omega)$ factor outside the inner sum,

$$\chi_{KS}(\omega,\bar{r},\bar{r}') = \sum_{k=1}^{P}\frac{4\overline{E}_k}{\omega^2-\overline{E}^2_k}\sum_{\varepsilon_{ia}\in I_k}\Theta_{ia}(\bar{r})\,\Theta_{ia}(\bar{r}'), \quad (15)$$

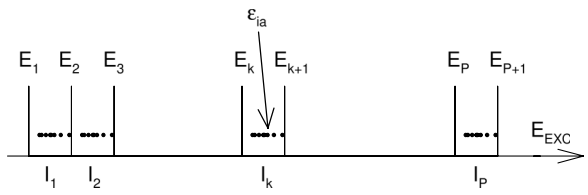

FIG. 1. Discretization of the energy axis to accommodate eigenvalue differences for the efficient calculation of the dielectric susceptibility. See text for details.

so in expression (15), the frequency dependent dielectric susceptibility is a linear combination of frequency independent objects (the inner sum) while only the coefficients are frequency dependent. Moreover, if one is interested in the lowest part of the spectrum as it usually happens, the sum in (15) can be safely truncated at a maximum energy cutoff, which can be chosen checking the convergence of the results with respect to such energy cutoff. This re-summation is the central idea of the present algorithm and is quite general irrespective to the introduction of the auxiliary basis set for the density fitting. We will now use this approach to build the matrix $\mathbf{M}(\omega)$. From Equation (11) and using expression (15), we get

$$M_{\mu\nu} = \sum_{k=1}^{P} s_k(\omega) \sum_{\varepsilon_{ia}\in I_k} \left\langle f_\mu \middle| \Theta_{ia}(\bar{r}) \right\rangle \left\langle \Theta_{ia}(\bar{r}') \right| K \left| f_\nu \right\rangle = \sum_{k=1}^{P} s_k(\omega) G^k_{\mu\nu}, \tag{16}$$

which, now justifies previous expression (12), defines the matrix $\mathbf{G}^k$ and the coefficients,

$$s_k(\omega) = \frac{4\overline{E}_k}{\omega^2 - \overline{E}_k^2}. \tag{17}$$

The construction of each $\mathbf{G}^k$ matrix corresponds to a matrix-matrix product,

$$G^k_{\mu\nu} = \sum_{\varepsilon_{ia}\in I_k} \left\langle f_\mu \middle| \Theta_{ia}(\bar{r}) \right\rangle \left\langle \Theta_{ia}(\bar{r}') \right| K \left| f_\nu \right\rangle = \sum_{\varepsilon_{ia}\in I_k} A^k_{\mu,ia} B^k_{ia,\nu}, \qquad \mathbf{G^k} = \mathbf{A}^k\mathbf{B}^k. \tag{18}$$

The matrices $\mathbf{A}$ and $\mathbf{B}$ must be built, formally with the following expansions:

$$A^k_{\mu,ia} = \left\langle f_\mu \middle| \varphi_i\varphi_a \right\rangle = \sum_{\sigma\tau}^{basis} \left\langle f_\mu \middle| \sigma\tau \right\rangle c_{\sigma i} c_{\tau a} \tag{19}$$

in expression (19), σ and τ refer to orbital basis functions and c are the molecular orbital expansion coefficients (KS eigenvectors).

The calculation of (19) would be far prohibitive, but in ADF, a very efficient "pair fitting" technique has been already developed, so the run of the basis indexes is not free but limited so that at least one basis function lies on the same center of the fit function. This step is the most expensive in the matrix construction. In expression (19), the integrals between a fit function and two basis functions are already available in ADF between primitive (not symmetrized) functions. Actually, we have also implemented the calculation of the $\left\langle f_\mu \middle| \sigma\tau \right\rangle$ integrals when the functions lie on three different centres. Since Slater type orbitals (STOs) functions are employed, these integrals are not analytical but can be easily calculated by fitting the products of two basis functions with the auxiliary density fitting functions. This does not change the dimension of Equation (9) but increases the computational effort to build matrix A^k (Equation (19)). However, we have noticed in preliminary test calculations that this does not change the results appreciably, and therefore, we have always neglected the $\left\langle f_\mu \middle| \sigma\tau \right\rangle$ integrals when the functions are on three different centres.

For the matrix $\mathbf{B}$, the procedure is the same

$$B^k_{ia,\nu} = \langle \varphi_i\varphi_a | \frac{1}{|\bar{r}' - \bar{r}''|} | f_\nu \rangle + \langle \varphi_i\varphi_a | \frac{\partial V_{XC}}{\partial \rho} | f_\nu \rangle. \tag{20}$$

The first term in (20) can be calculated using the Resolution of the Identity (RI),

$$\langle \varphi_i\varphi_a | \frac{1}{|\bar{r}' - \bar{r}''|} | f_\nu \rangle = \sum_{\gamma\eta} \left\langle \varphi_i\varphi_a \middle| f_\gamma \right\rangle S^{-1}_{\gamma\eta} \langle f_\eta | \frac{1}{|\bar{r}' - \bar{r}''|} | f_\nu \rangle = \left((\mathbf{A}^k)^+ \mathbf{S}^{-1} \mathbf{F} \right)_{ia,\nu}, \tag{21}$$

where in (21), the matrix $\mathbf{F}$ is defined as follows:

$$F_{\mu\nu} = \langle f_\mu | \frac{1}{|\bar{r}' - \bar{r}''|} | f_\nu \rangle. \tag{22}$$

The second term in (20) can be calculated in a similar fashion,

$$\langle \varphi_i\varphi_a | \frac{\partial V_{XC}}{\partial \rho} | f_\nu \rangle = \sum_{\gamma\eta} \left\langle \varphi_i\varphi_a \middle| f_\gamma \right\rangle S^{-1}_{\gamma\eta} \langle f_\eta | \frac{\partial V_{XC}}{\partial \rho} | f_\nu \rangle = \left((\mathbf{A}^k)^+ \mathbf{S}^{-1} \mathbf{Z} \right)_{ia,\nu}, \tag{23}$$

and the matrix Z in (23) is defined as follows:

$$Z_{\mu\nu} = \langle f_\mu | \frac{\partial V_{XC}}{\partial \rho} | f_\nu \rangle. \tag{24}$$

Equations (20), (23), and (24) are limited to ALDA and cannot be used in the present formulation for non-local kernels.

Therefore, from (20), (21), and (23), we get

$$\mathbf{B}^k = (\mathbf{A}^k)^+ \mathbf{S}^{-1} (\mathbf{F} + \mathbf{Z}). \tag{25}$$

Finally, from Equations (18) and (25),

$$\mathbf{G}^k = \mathbf{D}^k \mathbf{L}, \tag{26}$$

where the following two new matrices are introduced:

$$\mathbf{D}^k = \mathbf{A}^k (\mathbf{A}^k)^+, \tag{27}$$

$$\mathbf{L} = \mathbf{S}^{-1} (\mathbf{F} + \mathbf{Z}). \tag{28}$$

In practice, all the integrals (Equations (20)–(23)) needed to calculate the $\mathbf{G}^k$ matrices are already available in ADF, except the matrix Z (Eq. (24)) which has been implemented numerically. Then, each $\mathbf{G}^k$ matrix is calculated by expression (26).

We have still to calculate the $\mathbf{d}$ vector of Equation (10), i.e., the non-homogeneous term of Equation (9). Taking advantage of previously described technique, it is straightforward that

$$d_\mu = \langle f_\mu | \chi_{KS}(\omega) | z \rangle = \sum_{k=1}^{P} s_k(\omega) \times \sum_{\varepsilon_{ia}\in I_k} \left\langle f_\mu \middle| \Theta_{ia}(\bar{r}) \right\rangle \left\langle \Theta_{ia}(\bar{r}) \middle| z \right\rangle = \sum_{k=1}^{P} s_k(\omega) \sum_{\varepsilon_{ia}\in I_k} A^k_{\mu,ia} \langle \varphi_i | z | \varphi_a \rangle, \tag{29}$$

so vector $\mathbf{d}$ is easily calculated at each frequency as a linear combination of frequency independent vectors, accessible from $\mathbf{A}$ matrix and conventional dipole matrix elements.

Finally, the complex dynamic polarizability components are calculated as

$$\alpha_{zz}(\omega) = \int \rho_z^{(1)}(\omega,\bar{r})\, z d\bar{r} = \sum_\mu b_\mu \int f_\mu z d\bar{r} = \sum_\mu b_\mu n_\mu; \tag{30}$$

the vector **b** in (30) is the solution of Equation (9), and the elements of the **n** vector are integrals which are easily calculated analytically.

This step concludes the calculation of the dynamic polarizability and therefore of the spectrum and furnishes the first order TD density which can be used to analyze and rationalize the results. However, our goal is to get also a more complete analysis of the spectrum, namely, in terms of linear combination of one-electron excited configurations or in terms of TCM.[18] For this purpose, it is convenient to adopt the Modified Sternheimer Approach (MSA) formulation[27] of linear response, which furnishes the first order perturbation of the KS orbitals,

$$\begin{aligned}\left[H_{KS}^0 - \varepsilon_i - \omega\right]\varphi_i^{(1,-)} &= -V_{SCF}\varphi_i,\\ \left[H_{KS}^0 - \varepsilon_i + \omega\right]\varphi_i^{(1,+)*} &= -V_{SCF}\varphi_i.\end{aligned} \tag{31}$$

From the perturbed orbitals, the perturbed density is obtained as

$$\rho^{(1)} = 2\sum_i^{occ} \varphi_i \left(\varphi_i^{(1,-)} + \varphi_i^{(1,+)*}\right). \tag{32}$$

It is worth noting that, for convenience, the second inhomogeneous equation in (31) is actually the complex conjugate with respect to that reported in Ref. 27 for $\varphi_i^{(1,+)}$. Equations (31) and (32) were used in the past to calculate self-consistently the V_{SCF} via Equation (6) in old TDDFT implementations,[28–30] but in the present context, they are useful to easily get the analysis in terms of one-electron configurations. In fact, if the perturbed orbitals are expanded in terms of virtual KS orbitals, the term in brackets in Equation (31) is diagonal. Moreover, the V_{SCF} is already available from Equations (9) and (6), so the following equations are obtained:

$$\begin{aligned}\left[\varepsilon_a - \varepsilon_i - \omega\right] c_i^{a-} &= -\langle\varphi_a| V_{SCF} |\varphi_i\rangle,\\ \left[\varepsilon_a - \varepsilon_i + \omega\right] c_i^{a+*} &= -\langle\varphi_a| V_{SCF} |\varphi_i\rangle.\end{aligned} \tag{33}$$

The polarizability is then expressed by

$$\begin{aligned}\alpha_{zz}(\omega) &= 2\sum_i^{occ}\sum_a^{virt} \langle\varphi_i| z |\varphi_a\rangle \left(c_i^{a-} + c_i^{a+*}\right)\\ &= \sum_i^{occ}\sum_a^{virt} \langle\varphi_i| z |\varphi_a\rangle P_i^a;\end{aligned} \tag{34}$$

the density matrix (dipole amplitudes) P_i^a is introduced in (34). From Equation (33) and using the definition of $s_k(\omega)$ (Equation (18)), we obtain

$$P_i^a = s_k(\omega)\langle\varphi_i| V_{SCF} |\varphi_a\rangle. \tag{35}$$

In practice, the absorption spectrum is obtained from the imaginary part of Equation (34) (like in expression (30)), and therefore, the analysis in terms of one-electron excited configuration and TCM is obtained from imaginary part of expression (35).

Using Equations (6) and (28), dipole amplitudes are actually calculated as follows:

$$P_i^a = s_k(\omega)\left[\langle\varphi_i| z |\varphi_a\rangle + \sum_{\mu\tau}^{fit} \left(A^k\right)_{ia,\mu}^{+} L_{\mu\tau} b_\tau\right]. \tag{36}$$

III. COMPUTATIONAL DETAILS

The method has been implemented in a local version of the ADF code, and more precisely, ADF has been modified in order to save on external files, all the needed integrals, and matrix elements, which were already calculated by ADF with the only exception of matrix Z (Equation (24)); this matrix has been implemented by the Gaussian numerical integration scheme of ADF. Then, a new program (independent by ADF) reads the files, builds all the needed matrices, solves TDDFT equation (9), calculates the spectrum, and performs the analysis. We have decided to implement the new code in a separate program independent by ADF in order to exploit more easily the parallelization, with the goal to obtain a code which was massively parallel and easily portable on different architectures. For this reason, we have used standard MPI and ScaLAPACK libraries. However, the inclusion of the complete program within ADF is under consideration and will be available in a future release of ADF.

In all calculations, we have employed the LB94 exchange-correlation model potential[31] to obtain the KS orbitals and eigenvalues from the KS equations, while the exchange-correlation kernel is approximated by ALDA[25] in the TDDFT part taking the derivative of the Vosko Wilk Nusair (VWN)[32] LDA XC potential. The basis sets employed consist of STOs included in the ADF database, as well as the auxiliary density fitting functions. The new program allows a simple choice of a subset of the ADF fitting functions, in order to save computer time when some fitting functions are not necessary for an accurate description of the photoabsorption spectrum. The strategy to choose a properly reduced fitting subset consists to perform some preliminary TDDFT test calculations on simple systems (for example, diatomic molecules) increasing gradually the number of fit functions. Typically, this procedure converges rather rapidly, giving calculated spectra that match better and better with that obtained with a standard TDDFT calculation by ADF. When a good match is obtained, the fitting subset of the corresponding atoms can be used for more complex or larger systems, as it will be shown in details in Sec. IV.

Equation (9) must be solved for each non-equivalent dipole component with the constraint that the integral of the induced density $\rho^{(1)}$ must be zero over space due to the orthogonality of occupied-virtual orbitals. This condition is naturally satisfied when the dipole component is not totally symmetric; on the other hand, when the system symmetry is low and one or more dipole components are totally symmetric, such constraint can be easily imposed by Lagrange multipliers after Equation (9) is solved. Most of the computational effort is spent in the resolution of complex algebraic linear system (9), which is managed by ScaLAPACK parallel library and should be portable on very large supercomputers.

While the ADF code fully exploits symmetry, this is only partially done in the present method: the density fitting basis functions are not symmetrised by now; however, only the pairs of occupied (φ_i) and virtual (φ_a) orbitals involved in allowed dipole selection rules are actually considered.

We have implemented the plasmon analysis in the present method according to Jacob *et al.*:[33] they suggested to study the evolution of the TDDFT photoabsorption spectra by changing a scaling factor $0 \leq \lambda \leq 1$ used to "turn on" the coupling matrix K. This can be easily done in present implementation multiplying the matrix **L** (Equation (28)) by the scaling factor λ. This scaling factor analysis has proven successful in previous studies on silver chains[34] and polyacenes.[35]

It is worth noting that the dynamic polarizability and therefore the spectrum can be in principle calculated equivalently by expression (30) or (34); however, we have found that expression (34) is much more accurate and less demanding in terms of density fitting size. This is not surprising since the dipole integrals in expression (34) are analytical while expression (30) requires a fitting able to accurately fit the occupied-virtual orbital product. For this reason, all the spectra reported in this work have been calculated with expression (34).

IV. RESULTS AND DISCUSSION

We have tested the performance of the new TDDFT algorithm implemented in this work, on a series of small but rather different systems (diatomic H_2, Na_2 Au_2, and triatomic H_2O) and finally on two rather large gold clusters Au_{86}[36] and $[Au_{147}]^-$.[37] The goal is to achieve a firm assessment of the accuracy of the method on small systems as well as of an accurate choice of the density fitting set. Finally, the large metal clusters have been selected since they have been already treated by standard TDDFT and offer therefore a good chance to compare the performances of the new method and test its numerical economy. It must be considered that the program is now installed only on a small HP ProLiant ML350p Gen8 server (with 16 cores Intel® Xeon® CPU E5-2650 2 GHz), on which the present calculations were run. The porting to a supercomputer and therefore the applications to much larger systems will be considered as the next step of a future work.

A. H_2

In Figure 2, we have reported the TDDFT photoabsorption spectrum of H_2 with the polarization along the bond, calculated by ADF and by present method employing a DZ basis set. An interatomic distance of 0.7414 Å has been used. The photoabsorption corresponds to the $1\sigma_g \rightarrow 1\sigma_u$ valence transition. In order to have an easier comparison between the results of the two algorithms, the discrete lines obtained by ADF have been convoluted by Lorentzian functions with Half Width Half Maximum (HWHM) $\eta = 0.3$ eV according to the following expression:

$$f(\omega) = \sum_I^N \frac{\eta^2 f_I}{(\omega - \omega_I)^2 + \eta^2}. \quad (37)$$

ω_I and f_I in (37) are the excitation energies and oscillator strengths, respectively, while the presence of η^2 in the numerator guarantees that the maximum of the Lorentzian for $\omega = \omega_I$ corresponds to the value of f_I when only one line is present. For the new algorithm, the imaginary part of the polarizability is calculated by Equation (34) for complex photon energy and in Figure 2, the plotted curves correspond to

$$f(\omega_r) = \frac{2\omega_r\omega_i}{3}\mathrm{Im}\left[\alpha(\omega)\right]. \quad (38)$$

ω_r and ω_i in (38) are the real and the imaginary part of the photon energy, respectively, and it must also be $\omega_i = \eta$ in order to have the same convolution as in ADF.

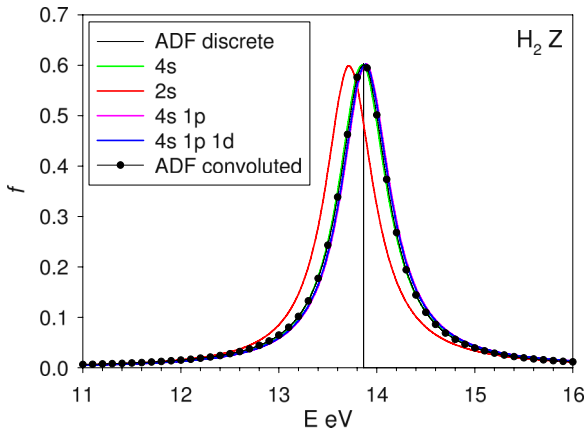

FIG. 2. Calculated TDDFT valence photoabsorption spectra of H_2 for polarization along the bond (Z direction). ADF results compared with present algorithm with various choices for the auxiliary basis for the density fitting.

An excellent agreement between the two methods emerges from the figure. Four different curves have been obtained with the new algorithm employing different reduced density fitting sets in the TDDFT part. The ADF DZ density fitting set of H consists of 4s, 3p, 2d, 1f, and 1g Slater functions (39 in total), which is much larger than needed; in fact, the absorption is well described already with only 2 s fitting functions, with an error in the energy of the maximum of only 0.12 eV. The match is excellent with 4 s fitting functions both for energy and intensity. Already at this level, it is evident that fitting set can be strongly reduced with respect to the original one.

To check the algorithm performance also for the real part of the dynamic polarizability, the comparison with ADF is reported in Figure 3. The agreement is excellent and the new algorithm is very accurate to reproduce quantitatively the behaviour of the polarizability with only 4 s density fitting functions.

B. Na_2

H_2 is a very simple molecule, so it is important to test the algorithm on systems which become more and more complex in order to gradually identify possible pitfalls of the method and to get acquainted with its performances. In this respect, Na_2 is interesting because both s and p atomic functions are important to describe valence molecular orbitals; moreover, we have employed a DZP basis set in order to include also d functions in the calculation. An interatomic distance of 2.9997 Å has been used. The original density fitting set of ADF for Na consists of 88 functions (14s 7p 6d 2f 1g);

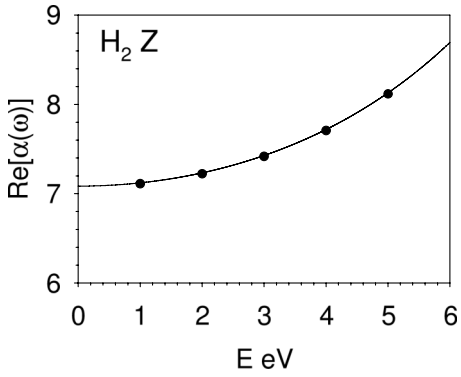

FIG. 3. Calculated TDDFT real part of the dynamical polarizability of H_2 for polarization along the bond (Z direction). ADF results (circles) compared with present algorithm (solid line).

after some preliminary test calculations, we have identified a much smaller set (7s 5p) containing only 22 functions which has been employed in the TDDFT calculation for Na_2 with the new algorithm.

The photoabsorption of Na_2 is considered in Figure 4, with convolution $\omega_i = \eta = 0.15$ eV and bond direction along the Z axis: the upper panel considers the photoabsorption with parallel polarization (along Z) and the lower panel with perpendicular polarization (along X). Taking into account, the electronic structure of Na_2,

$$(1\sigma_g)^2(1\sigma_u)^2(2\sigma_g)^2(2\sigma_u)^2(3\sigma_g)^2(3\sigma_u)^2(1\pi_u)^4(1\pi_g)^4 \times (4\sigma_g)^2(4\sigma_u)^0(2\pi_u)^0,$$

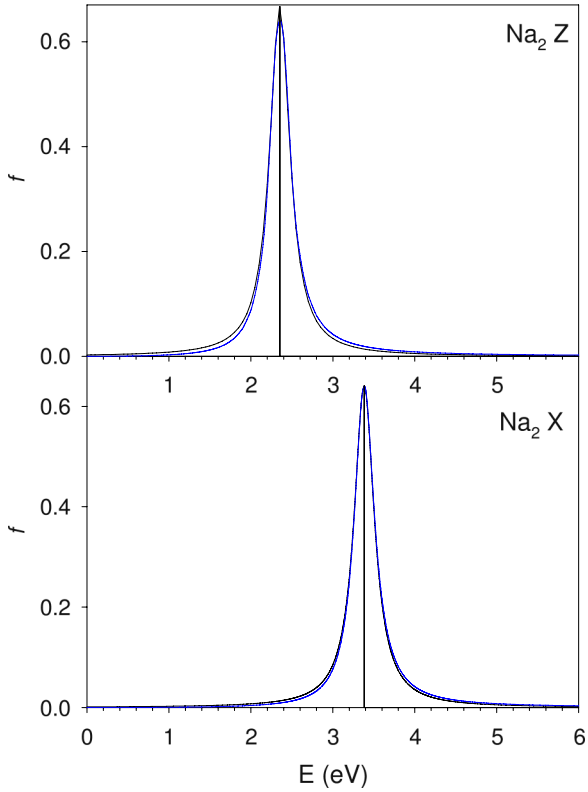

FIG. 4. Calculated TDDFT valence photoabsorption spectra of Na_2 for polarization along the bond (Z direction, upper panel) and perpendicular to the bond (X direction, lower panel). ADF results (black lines) compared with present algorithm (blue line).

the absorption with X polarization at 3.38 eV is ascribed to the $4\sigma_g \rightarrow 2\pi_u$ transition while the other one with Z polarization at 2.35 eV is ascribed to the $4\sigma_g \rightarrow 4\sigma_u$ transition. The match of the new algorithm with ADF is quantitative even with a fitting set which is 4 times smaller than the original one.

C. Au_2

We have considered gold dimer for two reasons: first its spectrum is quite complicated, with many transitions involving mixing of several one-electron excited configurations. The valence molecular orbitals are contributed by functions up to 4f and the density fitting set is quite rich, so its reduction must be carefully tested. Second, gold clusters are expected to be one of the most important applications of the present method in future works; therefore, it is very important to properly assess and to validate a robust choice of the density fitting for Au atom to be employed on larger systems.

The calculations have been performed at scalar relativistic level with Zero Order Relativistic Approximation (ZORA). The interatomic distance of 2.47 Å has been employed, and both DZ and TZ2P basis sets (with frozen core up to Au 4f) have been tested. The photoabsorption of Au_2 calculated with the DZ basis set is considered in Figure 5, with convolution $\omega_i = \eta = 0.30$ eV: the upper panel shows the photoabsorption with polarization parallel (Z) to the bond direction and the lower panel with perpendicular (X) polarization. The corresponding transitions calculated by ADF have been reported in Table I, together with their nature in terms of one-electron excited configurations. For the new algorithm, the density

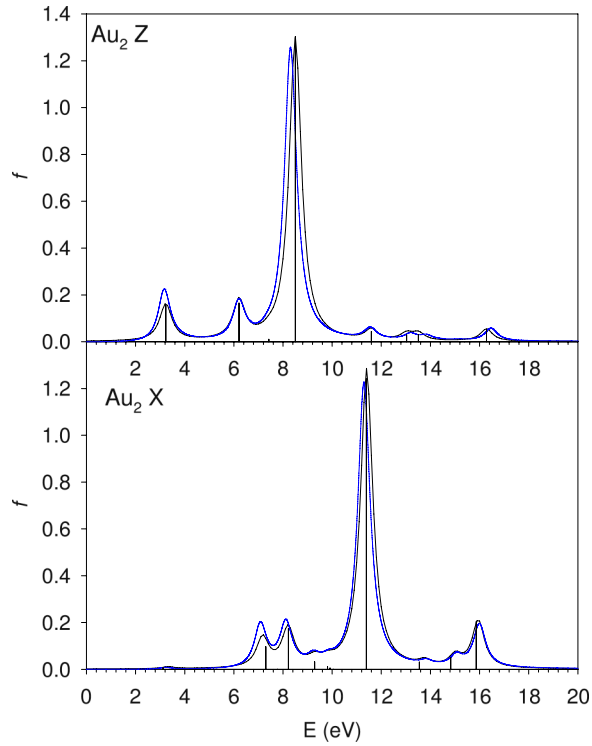

FIG. 5. Calculated TDDFT valence photoabsorption spectra of Au_2 for polarization along the bond (Z direction, upper panel) and perpendicular to the bond (X direction, lower panel) with DZ basis set. ADF results (black lines) compared with present algorithm (blue line).

TABLE I. Relevant TDDFT dipole allowed excitations of Au_2 (DZ basis set, LB94 potential, and ZORA scalar relativistic) calculated by ADF.

Transition	E (eV)	f	Assignment
$1\Sigma_u$	3.23	0.157	100% $14\sigma_g$ (86% 6s 14% $5d_{z^2}$) $\rightarrow 14\sigma_u$ (78% 6s 18% $6p_z$)
$3\Sigma_u$	6.21	0.165	78% $13\sigma_g$ (85% $5d_{z^2}$ 14% 6s) $\rightarrow 14\sigma_u$
$7\Sigma_u$	8.50	1.299	62% $8\pi_g$ (100% $5d_{xz}$) $\rightarrow 9\pi_u$ (100% $6p_{x,y}$) 17% $13\sigma_u$ (99% $5d_{z^2}$) $\rightarrow 15\sigma_g$ (95% $6p_z$)
$2\Pi_u$	7.30	0.097	69% $14\sigma_g \rightarrow 9\pi_u$ 28% $4\delta_g$ (100% $5d_{xy,x^2-y^2}$) $\rightarrow 9\pi_u$
$4\Pi_u$	8.22	0.174	62% $4\delta_g$ (100% $5d_{xy,x^2-y^2}$) $\rightarrow 9\pi_u$ 17% $14\sigma_g \rightarrow 9\pi_u$
$9\Pi_u$	11.40	1.241	44% $4\delta_u$ (100% $5d_{xy,x^2-y^2}$) $\rightarrow 9\pi_g$ (98% $6p_{x,y}$) 20% $13\sigma_u$ (99% $5d_{z^2}$) $\rightarrow 9\pi_g$ (98% $6p_{x,y}$)
$12\Pi_u$	15.87	0.204	98% $8\pi_g \rightarrow 16\sigma_u$ (84% $6p_z$)

fitting set has been reduced to 5s 4p 4d 1f for a total of 44 functions, with respect to the original set of 25s 15p 12d 8f 7g for a total of 249 functions, with a reduction of almost a factor of 6. Starting with the Z dipole absorption spectrum (Σ_u transitions), the most intense line is found at 8.50 eV; its nature consists in a mixing of two configurations: 62% $8\pi_g \rightarrow 9\pi_u$ and 17% $14\sigma_g \rightarrow 9\pi_u$, and the molecular orbitals involved are contributed by Au 5d and Au 6p for the initial and final states, respectively. The new algorithm simulates very well the ADF results in terms of intensity, although the excitation energy is underestimated by 0.2 eV. The other two transitions at lower energy are very well described in terms of excitation energy; the only observed discrepancy is a slight intensity overestimate of the band at 3.23 eV. Similar agreement is found for the X dipole component (subspecies of Π_u transitions), with only minor discrepancies in the intensity for the weaker transition at 7.30 eV and in the excitation energy of the transition at 11.40 eV an error of only 0.1 eV.

In Figure 6, the Z component has been calculated with the TZ2P basis set; a reduced density fitting set of 5s 4p 4d 1f 2g functions has been employed for the new algorithm. The quality of the agreement is comparable with that obtained with the DZ basis set, and it is worth noting that the main effect of an enlarged basis set in the ADF calculations consists in a shift to lower energy (by 0.5 eV at most) and a moderate intensity reduction. Both of them are very well reproduced by the new algorithm as well.

As a general statement, we can say that the new TDDFT complex polarizability algorithm performs very well on Au_2 if compared with the standard TDDFT Casida implementation of ADF, with expected deviations limited to few tenths of eV for the excitation energies and robust intensity reproduction and with modest deviations found for the weaker transitions.

D. H_2O

Water molecule has been calculated at DZP level. The absorption spectrum for both Y direction (in the molecular plane) and Z direction (C_2 axis) is considered in Fig. 7, with convolution $\omega_i = \eta = 0.30$ eV. The original density fitting auxiliary basis set for O atom, consisting of 68 functions (10s 5p 4d 2f 1g), has been reduced to 24 functions (2s 4p 2d) while for H atom; the original set of 39 functions (4s 3p 2d 1f 1g) has been reduced to 5 functions (2s 1p). Two transitions are found when the polarization is along Y (b_2), a weaker one at 12.63 eV ascribed to a 100% $3a_1 \rightarrow 2b_2$ transition, and a stronger one at 14.08 eV (100% $1b_2 \rightarrow 4a_1$). The spectrum calculated by complex polarizability algorithm is in good agreement with ADF for both transition energy (with deviations around 0.1 eV) and intensity; only for the weaker transition, the intensity appears slightly overestimated. When

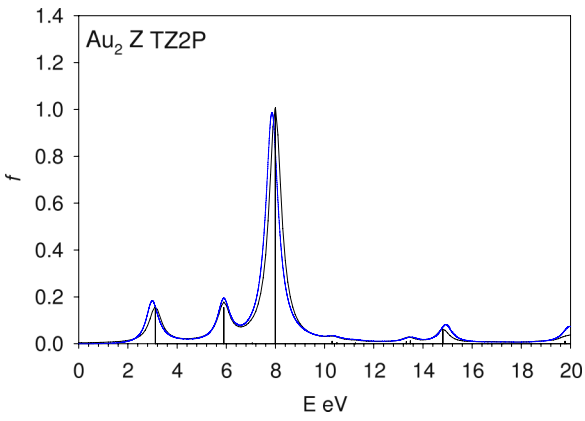

FIG. 6. Calculated TDDFT valence photoabsorption spectra of Au_2 for polarization along the bond (Z direction) with TZ2P basis set. ADF results (black lines) compared with present algorithm (blue line).

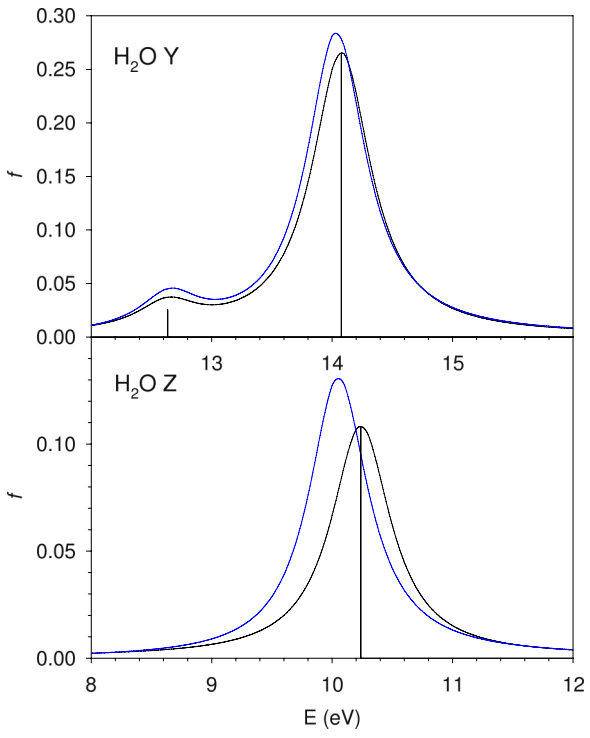

FIG. 7. Calculated TDDFT valence photoabsorption spectra of H_2O for polarization along the Y (upper panel) and Z (lower panel) directions. ADF results (black lines) compared with present algorithm (blue line).

the Z dipole component is considered, a single transition is found at 10.24 eV assigned as a 100% $3a_1 \rightarrow 4a_1$ excitation; this time the new algorithm overestimates the transition energy by 0.15 eV and the intensity by 10%. The discrepancies with respect to ADF are limited to 0.15 eV also for H_2O, and therefore, they are of the same size as found for previous biatomic systems.

E. Au_{86}

Since, up to now, the complex polarizability algorithm has been validated on simple small systems of different nature comparing individual transitions with respect to ADF, it is now necessary to assess its performances in terms of accuracy and computational economy also on larger systems, which we expect should represent the target of its future applications. We have taken into account first the Au_{86} gold nanowire, which has been already considered in our previous work, employing a DZ basis set and LB94 exchange correlation potential and displays a strong longitudinal plasmon around 2.35 eV.[36] Plasmons are photoabsorption features which start to appear when the metal (typically gold or silver) cluster size is beyond 2 nm for gold and are associated to free (collective) oscillations of the conduction band electrons and give rise to the so-called Surface Plasmon Resonance (SPR). Note that the longitudinal size of Au_{86} is 2.59 nm.

In Figure 8, the calculated spectra with both ADF and complex polarizability methods are compared: the new algorithm performs very well and the maximum absorbance at 2.35 eV is quantitatively reproduced. Moreover, it allows to calculate the spectrum at higher energy. In the figure, we have reported the photoabsorption up to 5 eV calculated truncating the expression of Equation (15) with an energy cutoff of 7 eV, a value which is high enough to display the opening of the deeper excitations arising from the Au 5d band, which start to show up around 4.5 eV. In the inset of the upper panel, we reported a sketch of an isosurface of the imaginary part of the perturbed density, calculated from the **b** vector solution of Equation (8) at 2.35 eV: the dipolar shape is indicative of a typical plasmonic behaviour. Its nature can be further analysed by means of the TCM plot reported in the lower panel of Figure 8: the "spots" are indicative of contribution from one-electron configuration associated with a pair of orbital energies (occupied on the X axis (ε_i) and virtual on the Y axis(ε_a)). The solid black diagonal line corresponds to an eigenvalue difference equal to the excitation energy (2.35 eV) while the dashed black diagonal line corresponds to the maximum (cutoff) energy of 7 eV presently considered in sum (15), corresponding to the E_{P+1} knot in Figure 1. In order to properly discuss TCM and extract maximum information from it, it is useful to analyze the KS electronic structure of such cluster: the Fermi energy is at −10.02 eV, and the s band lies in the interval from −11 to −10 eV, while the d band is mainly located below −12 eV for occupied orbitals, while virtual orbitals are all mixed 6s-6p, with 6p contribution gradually increasing with energy. The maximum contribution to the absorption is given by intraband 6s → 6s 6p transitions, in line with strong plasmonic behaviour, while the 5d → 6s 6p contribution is very low. It is well known that the plasmon intensity of gold is screened

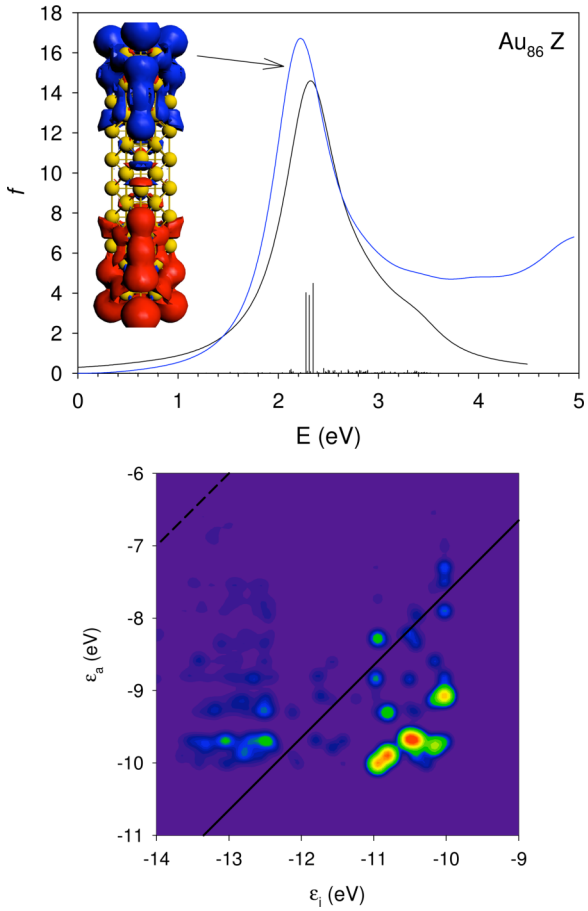

FIG. 8. Calculated TDDFT valence photoabsorption spectra of Au_{86} for polarization along the longitudinal direction (upper panel). ADF results (black lines) compared with present algorithm (blue line), inset: imaginary induced density at 2.35 eV. Lower panel: TCM analysis at 2.35 eV, x and y axes refer to occupied and virtual eigenvalues, respectively.

by intraband 5d → 6s 6p response,[18] such screening is weak in present case, and therefore, the plasmon gains intensity and appears rather strong. The TCM analysis is also very useful since it shows that the contributions from energy configurations decrease rapidly as the difference between the occupied-virtual eigenvalues moves away from the excitation energy (solid line), so the cutoff at 7 eV is justified *a posteriori*. Of course, if one would be interested to analyse the spectrum also above the plasmon, such cutoff should be shifted at higher and higher energy. However, the TCM analysis allows easily to check if the cutoff has been properly chosen or needs to be further shifted at higher energy. It is worth noting that if very high excitation energy were considered, a lower cutoff would be chosen as well, for example, in the case of core electron excitations.[38]

F. $[Au_{147}]^-$

In Au_{86}, the plasmon is very strong because the long longitudinal cluster size (2.59 nm) allows the collective effects to be prevailing with respect to the screening of the Au 5d band. However, if the cluster is larger but more spherical, the plasmon is less easy to be identified, due to its lower intensity and also because it is overwhelmed by the very intense

5d → 6s 6p interband transitions. For this reason, we have considered the $[Au_{147}]^-$ cluster in a previous study,[37] whose structure was optimized starting by from an icosahedral symmetry with a D_{5d} symmetry constraint, the relaxed structure was only slightly distorted with respect to *Ih*. The negative charge is chosen in order to have a closed-shell electronic structure. Due to the relaxed reduced D_{5d} symmetry constraint, the dipole allowed symmetries are A_{2u} and E_{1u} and the absorption spectrum is their sum. Since we are interested to compare the present complex polarizability algorithm with respect to ADF, we have limited the analysis to the A_{2u} symmetry alone; since for such representation, it is possible to extract safely 300 roots up to 3.78 eV, while for the E_{1u} one, it has proven impossible to reach such excitation energy due to the already mentioned problems of the Davidson algorithm. The results concerning the only A_{2u} dipole component are reported in Figure 9; it is worth noting that all the spectral features calculated by ADF (in particular the maximum at 3.45 eV) are very well reproduced by the new algorithm in terms of excitation energy, while the intensity is overestimated by a factor of two. It is worth noting, however, that the complex polarizability includes excitations up to 7 eV, so we attribute the disagreement to a kind of "background" intensity deriving from the "tail" of the higher energy excitations, which is correctly included

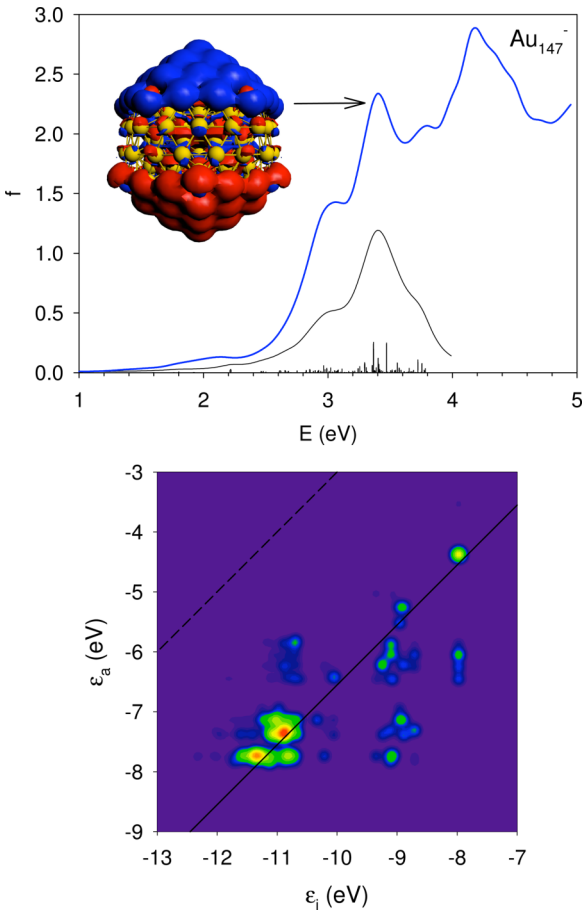

FIG. 9. Calculated TDDFT valence photoabsorption spectra of D_{5d} $[Au_{147}]^-$ for polarization along the C_5 axis (A_{2u} dipole component). ADF results (black lines) compared with present algorithm (blue line), inset: imaginary induced density at 3.45 eV. Lower panel: TCM analysis at 3.45 eV, x and y axes refer to occupied and virtual eigenvalues, respectively.

in the complex polarizability but is missing in ADF. In this case, we have also tested if the calculation of the $\langle f_\mu | \sigma\tau \rangle$ three centres integrals of Equation (19) would have improved the agreement between ADF and the new complex polarizability algorithm. However, also in this case, the contribution of the three centres integrals has proven irrelevant, so this approximation is not the origin of the found disagreement. The inset in the upper panel refers to the induced density calculated at the photon energy of the maximum. Also in this case, a typical dipolar shape is obtained, as expected for a SPR. In general, it is not easy to identify, with other computational schemes, a weak spectral feature like the present one at 3.45 eV over a monotonic increasing background, since it may happen that the resonant intensity is washed up and becomes confused with the background. For example, the truncated octahedral Au_{140} cluster did not show any feature at TDDFT level calculated with a time-evolution algorithm, although a weak plasmon would have been expected.[9]

In the lower panel of Figure 9, the TCM analysis is reported, performed at a photon energy of 3.45 eV which corresponds to the maximum of absorption. In this case, the Fermi energy is at −7.90 eV, the Au 6s band lies between −9 and −8 eV, and the Au 5d lies between −10 eV and −12 eV for occupied orbitals while virtual orbitals are all of mixed 6s-6p nature. This time, the leading contributions come from the intraband Au 5d → Au 6s 6p configurations (around −11 eV in the occupied eigenvalues scale) and from the Au 6s → Au 6s 6p ones (around −8 eV in the occupied orbital scale), both of them are placed very near to the diagonal corresponding to the eigenvalue difference equal to 3.45 eV. At variance with Au_{86}, in $[Au_{147}]^-$, the plasmon appears damped by the strong screening from the intraband Au 5d → Au 6s 6p response. Such TCM analysis is consistent with the ADF one: such comparison is relatively easy in this case because in ADF there are two lines at 3.37 eV and 3.47 eV which are much more intense than the other ones, so analysis can be restricted only to these lines. In other circumstances, namely, when one band corresponds to the convolution of many transitions of comparable intensity, TCM is much more convenient, since it can be performed by just taking the excitation energy of the maximum. On the other hand, in ADF, such situation would be almost impracticable, since one should analyse one by one, all the transitions which lie in the energy interval centred on the band maximum with wideness comparable to the FWHM employed for the convolution.

The plasmonic nature of the absorption can be also investigated by means of the scaling factor method suggested by Jacob,[33] which consists to follow the excitation energies evolution with respect to the scaling factor λ (as outlined in previous Sec. III): plasmonic excitations are characterized by a strong sensitivity of the excitation energy with respect to λ. In Figure 10, we have reported such analysis for both Au_{86} and $[Au_{147}]^-$, calculating the spectra with λ from 0 to 1 with step 0.2. The position of the maximum changes dramatically with respect to λ, in particular the maximum shifts to higher energy by 0.6 eV in $[Au_{147}]^-$ and by 0.4 eV in Au_{86} on going from λ = 0 to λ = 0.2. Interestingly, the energy shift is followed by a strong intensity reduction for the former and by a substantial intensity conservation for the latter.

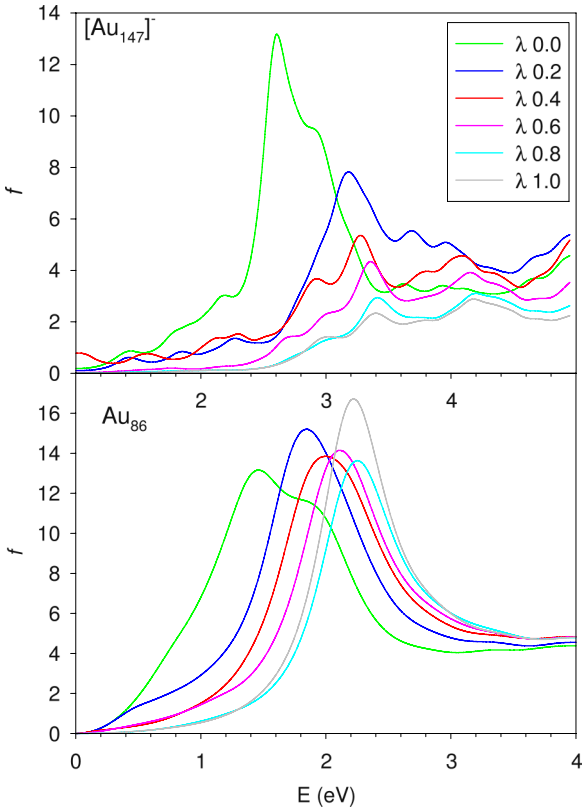

FIG. 10. Plasmon analysis according to Jacob. Upper panel: D_{5d} $[Au_{147}]^-$ (A_{2u} dipole component) and lower panel: Au_{86} longitudinal dipole component. Spectra calculated with present complex polarizability algorithm with different values of scaling factor parameter λ.

Due to the Thomas–Reiche–Kuhn (TRK) sum rule which states that the integral of oscillator strengths over the whole electronic spectrum must be equal to the number of electrons, we expect that the intensity for $[Au_{147}]^-$ will show up at higher energy.

V. CONCLUSIONS

In this work, we have developed and implemented a new algorithm within the ADF code, to solve the TDDFT equations in the space of the density fitting auxiliary basis set. The method extracts the spectrum from the imaginary part of the polarizability at any given photon energy, so the numerical part consists to solve a non-homogeneous system of linear algebraic equations, which can be managed by ScalaPACK parallel library, avoiding the bottleneck of Davidson diagonalization. The original idea, which makes the present scheme very efficient, consists in the simplification of the double sum over occupied-virtual pairs in the definition of the dielectric susceptibility, allowing an easy calculation of such matrix as a linear combination of constant matrices with photon energy dependent coefficients. The method has been applied to very different systems in nature and size (from H_2 to $[Au_{147}]^-$) in order to gain a global sensitivity about its accuracy and efficiency. In all cases, the maximum deviations observed with respect to ADF are below 0.2 eV, making the present algorithm a well balanced compromise, sacrificing some accuracy in favour of the efficiency and the capability to calculate the spectrum up to high energy together with wide analysis possibilities. In fact, the new algorithm has the merit not only to calculate the spectrum at whichever photon energy (at variance with the Casida formulation) but also to allow a deep analysis of the results, in terms of TCM, Jacob plasmon scaling factor, and induced perturbation analysis, which have been all implemented. Further applications to large non symmetric metal clusters are under study.

A possible extension of the method may include an automatic selection of the fitting functions, which must be done by the user at the moment.

It is worth noting that, although the point symmetry group is only partially exploited in the present implementation, the computational effort needed to treat large gold clusters has proven to be even lower than by ADF, which exploits instead the full symmetry. Therefore, we expect that the present scheme would be very efficient to treat also large systems with low symmetry, a typical situation met for metal clusters protected by ligands. In summary, we believe that the present method can represent a general and efficient way to apply TDDFT to very large systems, allowing specific applications on large metal clusters protected by ligands, which represents a rapidly developing field where theory can help to simulate optical properties of new materials and rationalize them in terms of electronic structure.

ACKNOWLEDGMENTS

The authors are grateful to Alessandro Fortunelli, Daniele Toffoli, Stan van Gisbergen, and Erik van Lenthe for fruitful discussions. Computational support from CINECA supercomputing centre within the ISCRA programme is gratefully acknowledged. This work has been supported by MIUR (Programmi di Ricerca di Interesse Nazionale PRIN 2010) of Italy and by FRA 2012 and FRA 2014 (Fondi di Ricerca di Ateneo) of University of Trieste.

[1]M. E. Casida, in *Recent Advances in Density-Functional Methods*, edited by D. P. Chong (World Scientific, Singapore, 1995), p. 155.
[2]E. J. Baerends, D. E. Ellis, and P. Ros, Chem. Phys. **2**, 41 (1973).
[3]C. Fonseca Guerra, J. G. Snijders, G. te Velde, and E. J. Baerends, Theor. Chem. Acc. **99**, 391 (1998).
[4]S. J. A. van Gisbergen, J. G. Snijders, and E. J. Baerends, Comput. Phys. Commun. **118**, 119 (1999).
[5]R. Ahlrichs, M. Bär, M. Häser, H. Horn, and C. Kölmel, Chem. Phys. Lett. **162**, 165 (1989).
[6]K. Yabana and G. F. Bertsch, Phys. Rev. B **54**, 4484 (1996).
[7]M. A. L. Marques, A. Castro, G. F. Bertsch, and A. Rubio, Comput. Phys. Commun. **151**, 60 (2003).
[8]A. Castro, M. A. L. Marques, D. Varsano, F. Sottile, and A. Rubio, C. R. Phys. **10**, 469 (2009).
[9]H.-Ch. Weissker and C. Mottet, Phys. Rev. B **84**, 165443 (2011).
[10]X. López-Lozano, H. Barron, C. Mottet, and H.-C. Weissker, Phys. Chem. Chem. Phys. **16**, 1820 (2014).
[11]B. Walker, A. M. Saitta, R. Gebauer, and S. Baroni, Phys. Rev. Lett. **96**, 113001 (2006).
[12]B. Walker and R. Gebauer, J. Chem. Phys. **127**, 164106 (2007).
[13]D. Rocca, R. Gebauer, Y. Saad, and S. Baroni, J. Chem. Phys. **128**, 154105 (2008).
[14]P. Ghosh and R. Gebauer, J. Chem. Phys. **132**, 104102 (2010).
[15]S. Grimme, J. Chem. Phys. **138**, 244104 (2013).
[16]C. Bannwarth and S. Grimme, Comput. Theor. Chem. **1040**, 45 (2014).
[17]T. J. Zuehlsdorff, N. D. M. Hine, J. S. Spencer, N. M. Harrison, D. J. Riley, and P. D. Haynes, J. Chem. Phys. **139**, 064104 (2013).

[18]S. Malola, L. Lehtovaara, J. Enkovaara, and H. Häkkinen, ACS Nano **7**, 10263 (2013).
[19]M. Noda, K. Ishimura, K. Nobusada, K. Yabana, and T. Boku, J. Comput. Phys. **265**, 145 (2014).
[20]K. Iida, M. Noda, K. Ishimura, and K. Nobusada, J. Phys. Chem. A **118**, 11317 (2014).
[21]M. Pavanello, J. Chem. Phys. **138**, 204118 (2013).
[22]R. Kevorkyants, H. Eshius, and M. Pavanello, J. Chem. Phys. **141**, 044127 (2014).
[23]M. Valiev, E. J. Bylaska, N. Govind, K. Kowalski, T. P. Straatsma, H. J. J. van Dam, D. Wang, J. Nieplocha, E. Aprà, T. L. Windus, and W. A. de Jong, Comput. Phys. Commun. **181**, 1477 (2010).
[24]J. Kauczor, P. Jørgensen, and P. Norman, J. Chem. Theory Comput. **7**, 1610 (2011).
[25]E. K. U. Gross and W. Kohn, "Time-dependent density-functional theory," Adv. Quantum Chem. **21**, 255 (1990).
[26]A. Ipatov, A. Hesselmann, and A. Görling, Int. J. Quantum Chem. **110**, 2202 (2010).
[27]G. D. Mahan and K. R. Subbaswamy, *Local Density Theory of Polarizability* (Plenum Press, New York, 1990).
[28]M. Stener, P. Decleva, and A. Lisini, J. Phys. B: At., Mol. Opt. Phys. **28**, 4973 (1995).
[29]M. Stener and P. Decleva, J. Chem. Phys. **112**, 10871 (2000).
[30]M. Stener, G. Fronzoni, D. Toffoli, and P. Decleva, Chem. Phys. **282**, 337 (2002).
[31]R. Van Leeuwen and E. J. Baerends, Phys. Rev. A **49**, 2421 (1994).
[32]S. H. Vosko, L. Wilk, and M. Nusair, Can. J. Phys. **58**, 1200 (1980).
[33]S. Bernadotte, F. Evers, and C. R. Jacob, J. Phys. Chem. C **117**, 1863 (2013).
[34]B. Gao, K. Ruud, and Y. Luo, J. Phys. Chem. C **118**, 13059 (2014).
[35]L. Bursi, A. Calzolari, S. Corni, and E. Molinari, ACS Photonics **1**, 1049 (2014).
[36]G. M. Piccini, R. W. A. Havenith, R. Broer, and M. Stener, J. Phys. Chem. C **117**, 17196 (2013).
[37]N. Durante, A. Fortunelli, M. Broyer, and M. Stener, J. Phys. Chem. C **115**, 6277 (2011).
[38]J. Kauczor and P. Norman, J. Chem. Theory Comput. **10**, 2449 (2014).